catalysts

MDPI

Article

Computational-Designed Enzyme for β-Tyrosine Production in Lignin Valorization

Fei Peng, Habibu Aliyu, André Delavault, Ulrike Engel and Jens Rudat *

Institute of Process Engineering in Life Sciences, II: Technical Biology, Karlsruhe Institute of Technology, Fritz-Haber-Weg 4, 76131 Karlsruhe, Germany; fei.peng@kit.edu (F.P.); habibu.aliyu@kit.edu (H.A.); andre.delavault@kit.edu (A.D.); ulrike.engel@kit.edu (U.E.)

* Correspondence: jens.rudat@kit.edu; Tel.: +49-721-608-48428

Abstract: Lignin is an underutilized sustainable source of aromatic compounds. To valorize the low-value lignin monomers, we proposed an efficient strategy, involving enzymatic conversion from *trans-p*-hydroxycinnamic acids to generate valued-added canonical and non-canonical aromatic amino acids. Among them, β-amino acids are recognized as building blocks for bioactive natural products and pharmaceutical ingredients due to their attractive antitumor properties. Using computational enzyme design, the (*R*)-β-selective phenylalanine aminomutase from *Taxus chinensis* (TchPAM) was successfully mutated to accept β-tyrosine as the substrate, as well as to generate the (*R*)-β-tyrosine with excellent enantiopurity (ee > 99%) as the unique product from *trans-p*-hydroxycinnamic acid. Moreover, the kinetic parameters were determined for the reaction of four Y424 enzyme variants with the synthesis of different phenylalanine and tyrosine enantiomers. In the ammonia elimination reaction of (*R*)-β-tyrosine, the variants Y424N and Y424C displayed a two-fold increased catalytic efficiency of the wild type. In this work, a binding pocket in the active site, including Y424, K427, I431, and E455, was examined for its influence on the β-enantioselectivity of this enzyme family. Combining the upstream lignin depolymerization and downstream production, a sustainable value chain based on lignin is enabled. In summary, we report a β-tyrosine synthesis process from a monolignol component, offering a new way for lignin valorization by biocatalyst modification.

Keywords: β-tyrosine; β-amino acid; phenylalanine aminomutase; lignin valorization; computational enzyme design; Rosetta enzyme design

Citation: Peng, F.; Aliyu, H.; Delavault, A.; Engel, U.; Rudat, J. Computational-Designed Enzyme for β-Tyrosine Production in Lignin Valorization. *Catalysts* **2021**, *11*, 1310. https://doi.org/10.3390/catal11111310

Academic Editors: Sarah L. Montgomery and Wojciech Zawodny

Received: 30 September 2021
Accepted: 27 October 2021
Published: 29 October 2021

1. Introduction

1.1. Lignin Valorization

The consistent depletion of finite petroleum resources has excited the rising eagerness for new renewable materials in recent years [1]. Lignocellulosic biomass, a low-priced and abundantly available feedstock, has piqued researchers' curiosity around the globe on the development of strategies for the conversion into renewable products [2–4]. The primary components of lignocellulosic biomass are cellulose, hemicellulose, and lignin. Among them, cellulose and hemicellulose can be degraded into carbohydrates by hydrolysis and further converted to ethanol and other fine chemicals [5]. In contrast to the polysaccharides in lignocellulosic biomass, lignin is formed by cross-linked aromatic monolignol precursors in a heterogeneous network to provide terrestrial plants with mechanical support, facilitating the transport of water and nutrients and defense against various pathogen attacks [6]. Because of the complexity of the structure and the recalcitrance to degradation, lignin is usually released as a waste in the pulp and paper mill effluent or is simply burned for the production of heat and power. Currently, over 50 million tons of lignin are produced annually in global paper and bioethanol factories [7]. Numerous studies have been carried out on the development of lignin valorization to generate aromatic value-added products [8].

However, lignin is primarily recognized as a macromolecule in valorization strategy based on the growing mature depolymerization techniques. Although this strategy has been accomplished with numerous promising examples, such as carbon fibers [9], adhesives [10], emulsifiers [11,12], binders [13,14], and lignin-based nanoparticles [15], the valorization of low-molecular-weight and high-value chemicals from lignin with aromatic potential is still in the initial stage and remains a huge challenge. Only a few industrial-scale examples in these areas have been reported until now, for instance, ferulic acid and vanillin production [8,16,17]. Currently, more rewarding strategies are being developed depending on the technological advances in lignin valorization, including recovery, depolymerization, and conversion. The establishment of a sustainable value chain has gained much attention in the area of lignin valorization [18,19].

The monolignols of lignin, differing in their degree of methoxylation: *p*-coumaryl-, coniferyl-, and sinapyl alcohol, are synthesized from the phenylpropanoid pathway, especially under drought [20], salinity [21], and heat [22] stresses. Besides, another monomer in the phenolic acid form like *p*-hydroxycinnamic acid also drives lignin polymerization and regulates seeding growth and germination [23]. The distribution of these monolignols varies among plant species and tissue types, and development stages and growth conditions. For instance, *p*-hydroxycinnamyl alcohol, representing the typical monolignol in grasses in a small percentage, offers significant potential to form *p*-hydroxycinnamic acid, which could also be produced directly from base-catalyzed depolymerized lignin liquors [24]. Notably, *p*-hydroxycinnamyl alcohol, comprising around 30% of total lignin, is one of the dominant compounds in curaua leaf fiber [25].

1.2. β-Amino Acids and Anticancer Drugs

Cancer was responsible for approximately 10 million deaths in 2020, according to the WHO report [26]. With the increase in mortality rates of cancer and the associated socioeconomic burden, one of the prime requirements of anticancer drug research is the establishment of a more economic and effective strategy for their industrial-scale synthesis.

β-amino acids, as building blocks in natural products with an attractive antitumor feature, have gained considerable interest in the field of oncology drug development over recent years. As a consequence, numerous bioactive products with high pharmacological potency that contain optically pure β-amino acid are already available as anticancer drugs. For instance, the notable β-amino acid-involved anticancer agent C-1027 chromoprotein, isolated from *Streptomyces globisporus*, is assembled by a unique β-amino moiety, (*S*)-3-chloro-4,5-dihydroxy-β-phenylalanine [27]. Another example in the treatment of various types of cancers is paclitaxel (Taxol®), which was initially extracted from the bark of the Pacific yew tree, *Taxus brevifolia.* Paclitaxel, as an effective microtubule-stabilizing drug to induce mitotic arrest of cells, carries a β-phenylalanine-derivative (2*R*,3*S*)-phenylisoserine on the functionally essential C13-side chain [28,29].

Phenylalanine aminomutase (PAM; EC 5.4.3.10), catalyzing the rearrangement of the (*S*)-α-phenylalanine and (*R*)-β-phenylalanine, is the principal enzyme in the committed step of the *N*-benzol phenylisoserinoyl side chain in the taxol biosynthesis pathway, while tyrosine aminomutase (TAM; EC 5.4.3.6) catalyzes the formation of C-1027 from L-tyrosine [27–29]. Both of these enzymes are members of the MIO (3,5-dihydro-5-methylidene-4H-imidazole-4-one)-dependent aminomutase family. These so-called MIO-dependent aminomutases recruit an unusual highly electrophilic moiety MIO for catalyzing the 2,3-amine shift in aromatic amino acids and present outstanding enantioselectivity. The members from this enzyme family are frequently applied for an asymmetric synthesis route without cofactor recycling to produce the optically pure β-amino acids [30,31]. On the other hand, the enzymatic synthesis of optically pure β-amino acids has been considered as an attractive strategy, compared to the chemical processes, which are limited by low yield or enantiopurity, and high cost of the waste treatment. Among these MIO-dependent enzymes, PAM is presumably evolved in ancient gymnosperms from the ancestry with phenylalanine ammonia-lyase (PAL; EC 4.3.1.24), according to our previous conclusion from phylogenetic

analysis. Regulating the metabolite accumulation in the phenylpropanoid pathway, PAM could be employed as a connection point for conversion from monolignol to high-valued β-amino acids in the enzymatic lignin valorization strategy [32].

Enzyme design efforts relying on the screening of large mutant libraries have had noteworthy success in the last decades, but they are usually time- and cost-intensive by using wide-ranging random mutagenesis. Instead, computational methods have been developed to guide the selection of the target substrate of enzymes in a limited number. One of the most powerful model tools is PyRosetta, which was broadly used for enzyme design based on the binding energy calculation of small molecule–protein interaction [33]. Supported by the previous high-resolution X-ray structure analysis and site-directed mutagenesis studies, TchPAM was an enzyme with excellent enantioselectivity. Therefore, it was chosen for the biosynthesis investigation of β-tyrosine from *trans-p*-hydroxycinnamic acid. To avoid screening in the massive mutant libraries, TchPAM is designed using a computational program instead of random experimental evolution [34,35].

2. Results and Discussion

2.1. Computational Design of TchPAM for the Synthesis of β-tyrosine

Previous mutagenesis studies on MIO-dependent enzymes revealed that the responsible residues for the substrate selectivity were mainly placed around the aromatic side of the substrate [33]. The X-ray co-crystal structure of TchPAM with native substrate-bound (PDB ID: 4C5R) was investigated to identify the other potential residues for acceptance of β-tyrosine [34]. It was hypothesized that various residues in the active site of TchPAM orient and stabilize the aromatic ring of the substrate. Previous studies on the substrate spectrum of TchPAM revealed that this enzyme accepts a range of monosubstituted cinnamic acid derivatives, especially those with methyl groups at the *para*-position, such as 4-methoxycinnamic acid. Therefore, β-tyrosine with a 1,4-hydroxyl group is not accepted by this enzyme because of the electrostatic restriction instead of the steric constraint [36]. Excluding the essential residues for catalysis and stereoselectivity (Asn231, Gln319, Tyr322, Arg325, Asn355), the other residues were divided into two groups. Group one comprises residues like Phe86, Leu104, Cys107, Leu108, Leu179, Tyr424, Lys427, Ile431, and Glu455, which potentially interact with the phenolic side of β-tyrosine via a hydrogen bond. The second group includes residues, such as Asn458 and Gln459, which form a stable network with substrates. The former residues were customized to contain polar or electrically charged side chains, while the latter were randomly mutated in silico without any limitation (Figure 1). In conclusion, a library of variants with multiple mutations was established using Rosetta enzyme design based on the penalty score of the constraints and visual structure screening of the designed enzymes.

2.2. Experimental Screening of the Designed TchPAM Mutants

Initially, the single point mutants from the mutant library were selected to explore the correlation between the phenolic group of β-tyrosine and the residues in the active site of the enzyme. Unexpectedly, residue Leu107, which was considered as the crucial position for the selectivity switch between tyrosine- and phenylalanine ammonia-lyase activity, was excluded in this computational mutant library [36,37]. To determine the substrate tolerance of the designed mutants, the specific activity in ammonia elimination reactions of (*S*)-α-phenylalanine, (*R*)-β-phenylalanine, (*S*)-α-tyrosine, and (*R*)-β-tyrosine were measured (Figure 2).

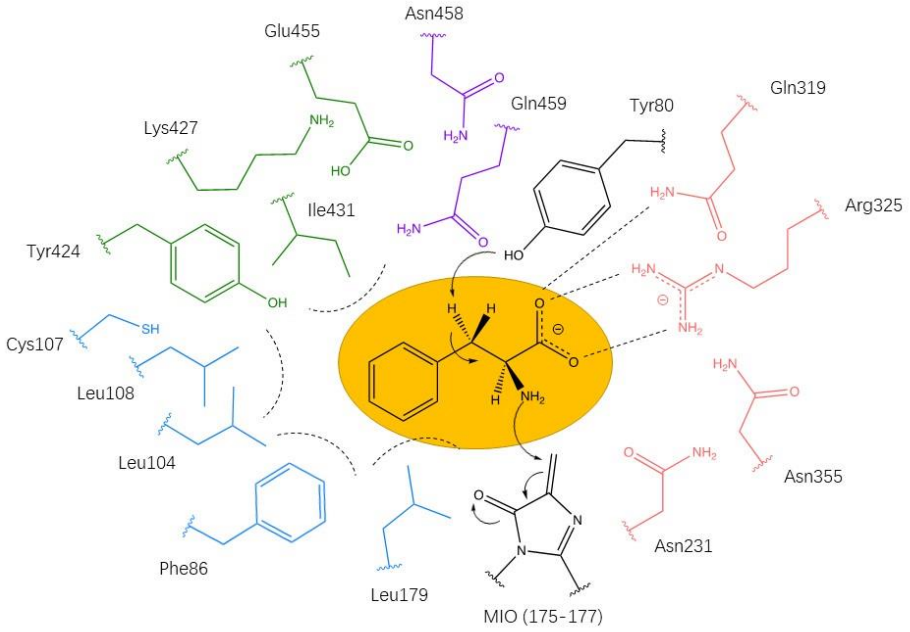

Figure 1. Schematic representation of the interactions between the natural substrate (*S*)-α-phenylalanine and TchPAM (PDB ID: 4C5R). The color coding corresponds to the position of residues in the active site: carboxyl binding pocket (red), aromatic binding pocket (blue), tyrosine towards pocket (green), essential functional residues (black), and all other residues without specified function (purple). The substrate (e.g., (*S*)-α-phenylalanine) is highlighted by a yellow background.

Tyr424Asn, the best variant of the library, shows the highest specific activity toward β-tyrosine and served not only to confer tyrosine acceptance but also to enhance the phenylalanine ammonia-lyase activity. An analogous outcome was observed in Tyr424Cys, but with a lesser activity improvement, compared to the wild type and the other variants (Tyr424Asp and Tyr424Gln). In the wild type, it was hard to form an interaction due to the distance of above 8 Å between the ring centroids from Tyr424 and the aryl-ring on the substrates. The mutant Tyr424Cys has a similar but more flexible conformation in the active site. Although, the partial negatively charged sulfur group on the side chain could interact with the positive charge on the edge of the aromatic ring within a certain distance, there are fewer steric effects by cysteine than tyrosine at this position. This hypothesis is supported by their comparable activity toward the deamination of various substrates [38]. However, mutation of the residue at position 424 to smaller amino acids mainly affects the orientation of the neighboring residues, such as Phe86 and Lys427, during protein folding (Figure 3). Asn or Gln, which were recognized as globally neutral amino acids, offered a partial positive charge on their formamide group when placed near the phenolic ring of the substrate and the residue Phe86. Therefore, these residues could provide an attractive interaction with the ring center (Figure 3B,D) [38–40]. Notably, their amino groups were closer to the aromatic ring than their carbonyl groups, thereby increasing the electrostatic contribution. The functional group on position 424 resulted in a potential variety of conformation and geometrical constraints with its neighboring residues, especially in the case of Gln with a larger side chain [41]. Unlike the glutamine at this position, the mutant Tyr424Asn might have less or no influence on the substrate binding, considering the distance (5.7 Å) between the amide group and the centroid ring. Replacement of the tyrosine with negatively charged aspartic acid at this position generates a slightly repulsive force toward the negatively charged ring center in the substrates [42]. Therefore, the docking location of the substrate was likely more distant from this residue than the wild type (Figure 3). Moreover, the carboxyl group of the residue Tyr424Asp might interact with the amino group of its neighboring residue Lys427, which was stabilized by the carboxyl group from the residue Glu455. It might be a possible reason for partial activity

loss in mutant Tyr424Asp. In addition, both neighboring residues Lys427 and Glu455 were suggested to be catalytically essential positions in TchPAM, because their variants abolished the activity by using all four substrates. The other neighboring residue Ile431, however, seemed to strictly require a hydrophobic group since the variants harboring mutations to Asn or Glu lost complete activity. Consequently, the residue Tyr424 might influence the substrate positioning through the interaction of its side chain with the aryl ring on the aromatic amino acids. Moreover, the neighboring residues in this area play an important role in substrate positioning.

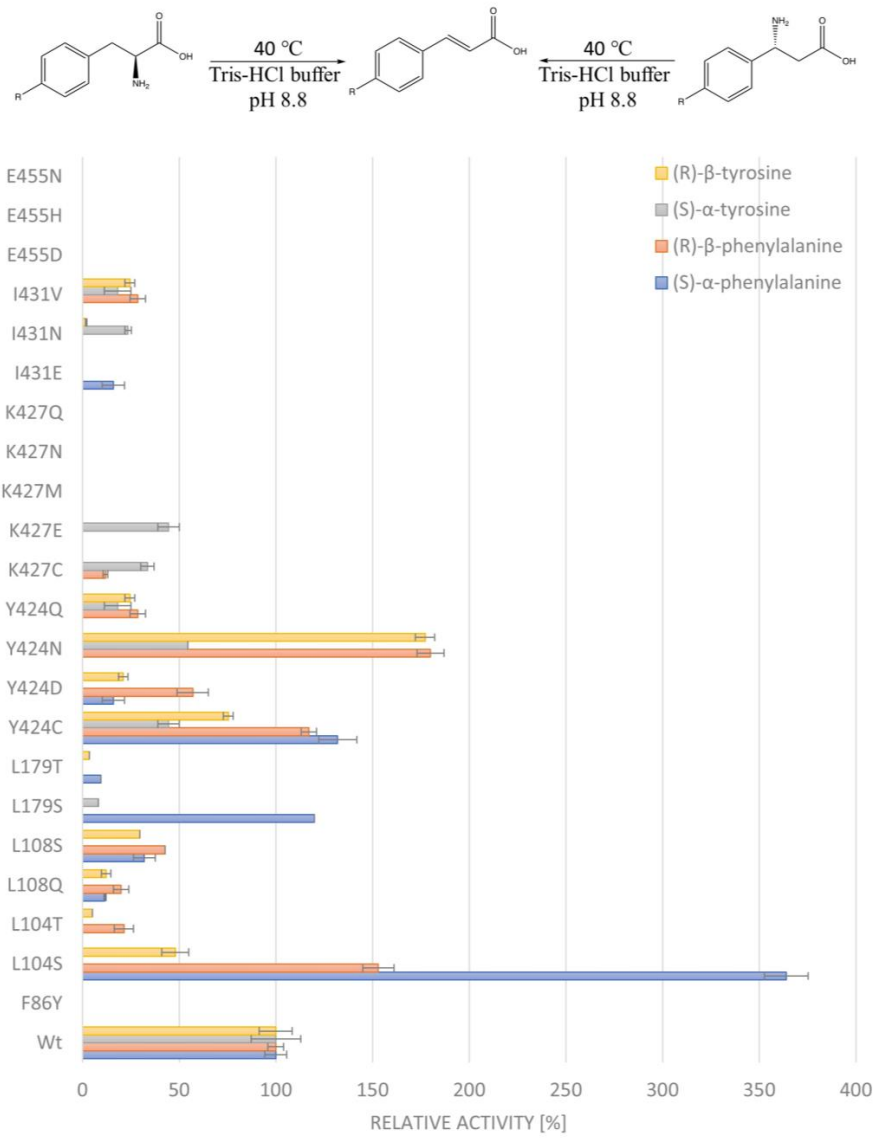

Figure 2. Deamination of different aromatic amino acids as a substrate for cinnamic acid or p-hydroxycinnamic acid by the mutant candidates from the computationally designed library. No activity was detected in the mutants without bars.

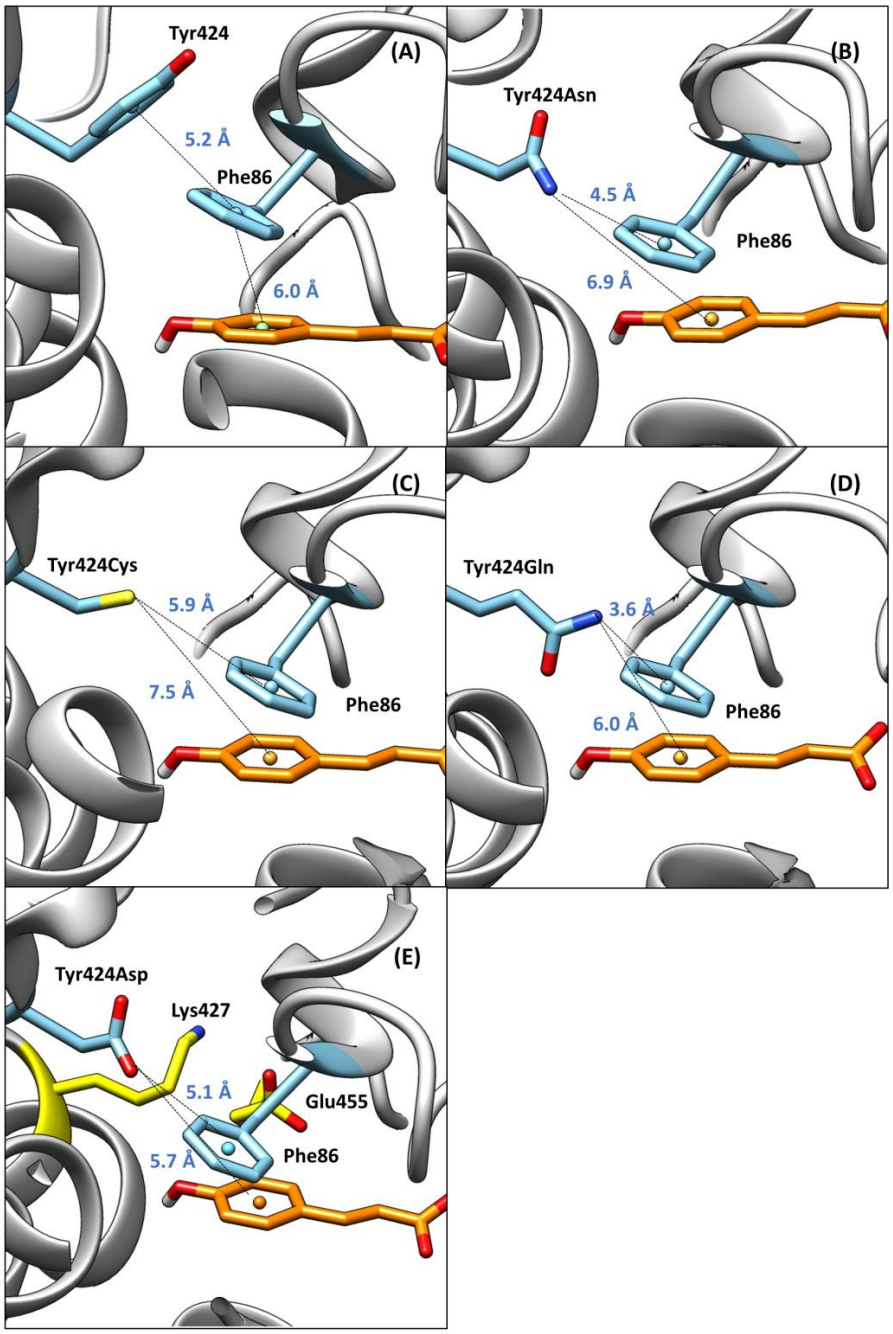

Figure 3. The docking structures with bound cinnamic acid as ligand in (**A**) the wild type, (**B**) the mutant Tyr424Asn, and (**C**) Tyr424Cys, (**D**) Tyr424Gln, and (**E**) Tyr424Asp. The residues are located above the aryl ring.

According to the amino acid sequence analysis, Phe86 was naturally replaced by tyrosine in the other MIO-dependent enzymes, which could accept tyrosine as substrates. However, the lack of activity in the Phe86Tyr variant indicated that the aromatic pair interaction between residue Phe86 and the benzyl or phenolic ring from the substrate probably induces a π–π interaction. This interaction helps to orient and stabilize the substrates in the wild type. Usually, this interaction could be observed at a pairing distance larger than 3.8 Å in slipped face-to-face stacking. The tyrosine variants increased the interaction by the withdrawing π-electron density from the hydroxyl group, resulting in a reduction of the electrostatic repulsion and the contact distance between the aromatic ring of residue Phe86Tyr and substrate [43,44]. As the other high-profile candidate residue

Leu108, which was considered as the responsible residues for α-tyrosine acceptance in the enzyme, did not seem to have the equivalent substrate-switching ability toward its β-isomers [37]. By replacing the residue Leu108, the mutants Leu108Gln and Leu108Ser were considerably less active toward both phenylalanine and tyrosine. In the former, the residue glutamine with the large side chain was more sterically hindered than leucine in the wild type, which could explain the notable activity decrease. On the other hand, the hydroxyl group on residue serine contributed to the strength of interaction with the sulfur atom from its nearby neighboring residue Cys107, giving a variant Leu108Ser with much lower activity.

The Leu104Ser variant was found to be the most efficient enzyme to catalyze the deamination of (*S*)-α-phenylalanine, giving an impressive 4-fold enhancement of specific activity, while the Leu104Thr, with a shorter polar uncharged side chain, lost most activity. This was consistent with the previous structural analysis of Leu104Ala, which was predicted to have an unfavorable steric strain between the residue and substituted cinnamic acid derivatives, especially at the *meta*-position. The same was observed when expanding the substrate scope of the MIO-dependent PcPAL from *Petroselinum crispum* [45,46]. It could be suggested that the residue Leu104 might influence the enzymatic catalysis due not only to the steric effect but also to the hydrophobic interaction between the residue and aromatic ring from the substrate.

2.3. Kinetic Analyses of Designed Enzymes

For Tyr424Asn and Tyr424Cys, the variants with enhanced substrate tolerance toward β-tyrosine, the kinetic parameters in the deamination reaction were determined, compared to the wild type and the other variants (Tyr424Asp and Tyr424Gln), which were mutated at the identical position (Table 1).

The kinetic data revealed that both variants with higher activity had an improved catalytic efficiency with tyrosine and a decreased catalytic efficiency with phenylalanine. Regarding β-tyrosine, the catalytic efficiency of Tyr424Cys and Tyr424Asn were 0.281 ± 0.023 and 0.234 ± 0.013 mM^{-1} s^{-1}, respectively. The variant Tyr424Cys displayed an approximately two-fold decreased K_M value but a k_{cat} value similar to that of the wild type. This is supporting the hypothesis that the replacement of tyrosine with a shorter side chain of the residue at position 424 could afford additional space for binding the phenolic ring on the substrate (Figure 3), whereas Tyr424Asn provided a similar binding affinity (K_M) and a superior turnover rate (around two-fold enhancement). This might be due to the interaction between the phenolic ring from the substrate and the partial positively charged amino group on the mutated residue when the β-tyrosine entered the catalytic site. Apart from the variant Tyr424Asp with a five-fold decline in K_M for α-phenylalanine, all four mutations yielded a lower binding affinity for their natural substrates in both isomers. Especially, Tyr424Asn gave a massive 20-fold higher K_M value when using β-phenylalanine as the substrate. It could be suggested that the residue Tyr424 assisted to enhance phenylalanine acceptance because of its large enough and negatively charged side chain. Meanwhile, variants Tyr424Asn and Tyr424Cys with α-tyrosine showed a huge, approximately 7-fold decrease in K_M value compared to the wild type. Therefore, the Tyr424 residue was confirmed to be a responsible position for conferring tyrosine or phenylalanine acceptance.

Table 1. Comparison of the kinetic parameters of wild type and mutants Tyr424Asn, Tyr424Asp, Tyr424Cys, and Tyr424Gln in ammonia elimination of various substrates.

(*S*)-α-Phenylalanine			
TchPAM	**K_M (mM)**	**k_{cat} (s^{-1})**	**k_{cat}/K_M (mM^{-1} s^{-1})**
wt	0.032 ± 0.001	0.02 ± 0.001	0.625 ± 0.02
Y424C	**0.048 ± 0.006**	**0.024 ± 0.002**	**0.506 ± 0.041**
Y424D	n.d.	n.d.	n.d.
Y424N	**0.075 ± 0.001**	**0.03 ± 0.002**	**0.407 ± 0.019**
Y424Q	0.006 [1]	0.003 [1]	0.608 ± 0.095
(*R*)-β-Phenylalanine			
TchPAM	**K_M (mM)**	**k_{cat} (s^{-1})**	**k_{cat}/K_M (mM^{-1} s^{-1})**
wt	0.062 ± 0.012	0.026 ± 0.002	0.427 ± 0.078
Y424C	**0.110 ± 0.017**	**0.035 ± 0.004**	**0.320 ± 0.044**
Y424D	0.458 ± 0.091	0.024 ± 0.006	0.053 ± 0.006
Y424N	**1.266 ± 0.108**	**0.138 ± 0.002**	**0.109 ± 0.01**
Y424Q	0.422 ± 0.073	0.022 ± 0.005	0.053 ± 0.006
(*S*)-α-Tyrosine			
TchPAM	**K_M (mM)**	**k_{cat} (s^{-1})**	**k_{cat}/K_M (mM^{-1} s^{-1})**
wt	2.435 ± 0.160	0.029 ± 0.005	0.011 ± 0.002
Y424C	**0.347 ± 0.065**	**0.01 ± 0.002**	**0.03 ± 0.004**
Y424D	n.d.	n.d.	n.d.
Y424N	**0.330 ± 0.024**	**0.007** [1]	**0.021 ± 0.001**
Y424Q	n.d.	n.d.	n.d.
(*R*)-β-Tyrosine			
TchPAM	**K_M (mM)**	**k_{cat} (s^{-1})**	**k_{cat}/K_M (mM^{-1} s^{-1})**
wt	0.465 ± 0.008	0.06 ± 0.001	0.130 ± 0.01
Y424C	**0.299 ± 0.005**	**0.084 ± 0.007**	**0.281 ± 0.023**
Y424D	n.d.	n.d.	n.d.
Y424N	**0.480 ± 0.015**	**0.112 ± 0.003**	**0.234 ± 0.013**
Y424Q	0.142 ± 0.001	0.014 ± 0.001	0.098 ± 0.008

[1] The deviation is smaller as 0.001.

2.4. Enantioselectivity of Designed Enzymes

The wild type of TchPAM can produce (*R*)-β-phenylalanine with >99% enantiomeric excess by using *trans*-cinnamic acid as the substrate. This accounts for around 50% of the product mixture, where (*S*)-α-phenylalanine occupies the rest. However, the *trans-p*-hydroxycinnamic acid was not accepted by this enzyme [36]. As a rare (*R*)-selective phenylalanine aminomutase in nature, TchPAM presents outstanding potential for the production of enantiopure (*R*)-β-tyrosine. Until now, comparable enantioselectivity has not been observed in the wild type of another member from the MIO-dependent enzyme family in the bacterial kingdom, for instance, the enzyme KedY4 from *Streptoalloteichus sp.* and the enzyme CmdF *Chondromyces crocatus* [47,48]. In contrast, the OsTAM from *Oryza sativa*, the only example of (*R*)-selective tyrosine aminomutase with great enantioselectivity in the plant, which is the closest relative of TchPAM, is tricky to apply in *trans-p*-hydroxycinnamic acid production [49].

The previous X-ray crystal structure analysis and the site-directed mutagenesis studies in TchPAM gave the proposal of the isomerization mechanism for explaining the aminomutase activity, revealing two possible distinct binding modes of the carboxyl group on substrates. The ammonia 1,4-addition for the production of (*S*)-α-phenylalanine was carried out by forming a bidentate salt bridge between the carboxylate group on the substrate and the amino groups from residue Arg325. The Gln319 afforded an extra interaction with the hydrogen bond and contributes to the orientation of the substrate. In the case of conversion to the corresponding (*R*)-configured β-phenylalanine, the carboxyl group

was stabilized by a network of hydrogen bonds, created by Asn231, Arg325, and Asn355. During the whole catalytic process, the aryl ring from *trans*-*p*-cinnamic acid was locked in the aromatic binding pocket, which contained the residues Phe86, Leu104, Leu107, and Leu108, and was identified to play a crucial role in substrate selectivity in previous studies [33]. From a similar catalytical point of view, two binding conformations could be postulated, when *trans*-*p*-hydroxycinnamic acid entered the active site as a starting substrate. Compared to the natural substrate *trans*-cinnamic acid, the ammonia addition of *trans*-*p*-hydroxycinnamic acid was difficult due to the substituted hydroxyl group of the benzenic ring. More electronegative oxygen atom shifts the electron to itself, stabilized by the negatively charged electron-withdrawing group, thus leading to the priming for nucleophilic attack at the β-position (Figure 4) [50]. Unlike the aryl ring from *trans*-cinnamic acid, which was stabilized in the aromatic binding pocket (Leu104, Leu108, and Leu179) by London dispersion force, the aryl ring from the *trans*-*p*-hydroxycinnamic acid oriented towards the residues with a polar or charged side chain (Cys107, Tyr424, Lys427, and Glu455) that could be attributed to its hydroxyl functional group (Figure 5). Of these two mentioned binding conformations of the carboxylate group on the substrate, only one would be favored in general. In this situation, the negatively charged carboxylate on *p*-hydroxycinnamic acid was preferred to stabilize in the latter binding mode, involving the hydrogen bonding formed by Asn231, Arg325, and Asn355, leading to the production of (*R*)-β-tyrosine. It could be strongly supported by the huge difference in the binding affinity for (*S*)-α-tyrosine and (*R*)-β-tyrosine in the wild type (Figure 5C,D). At this moment, the substrate backbone is placed closer to the carboxyl binding pocket, compared to the (*S*)-α-regioisomer (Figure 5A,B).

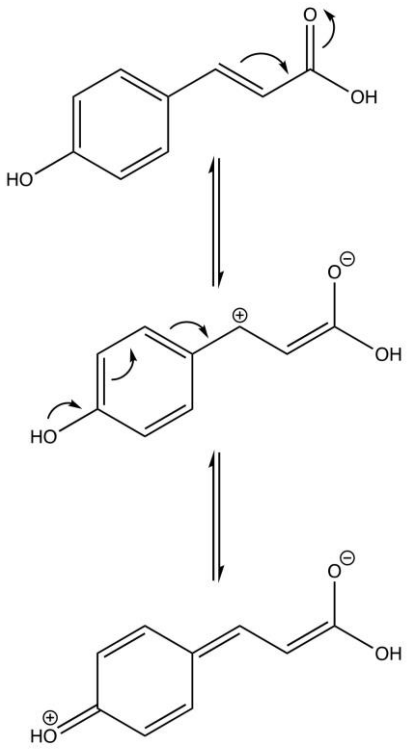

Figure 4. Resonance effect of the aromatic ring on *trans*-cinnamic acid to activate the β-position of the *trans*-*p*-hydroxycinnamic acid for the 1,4-nucleophilic addition.

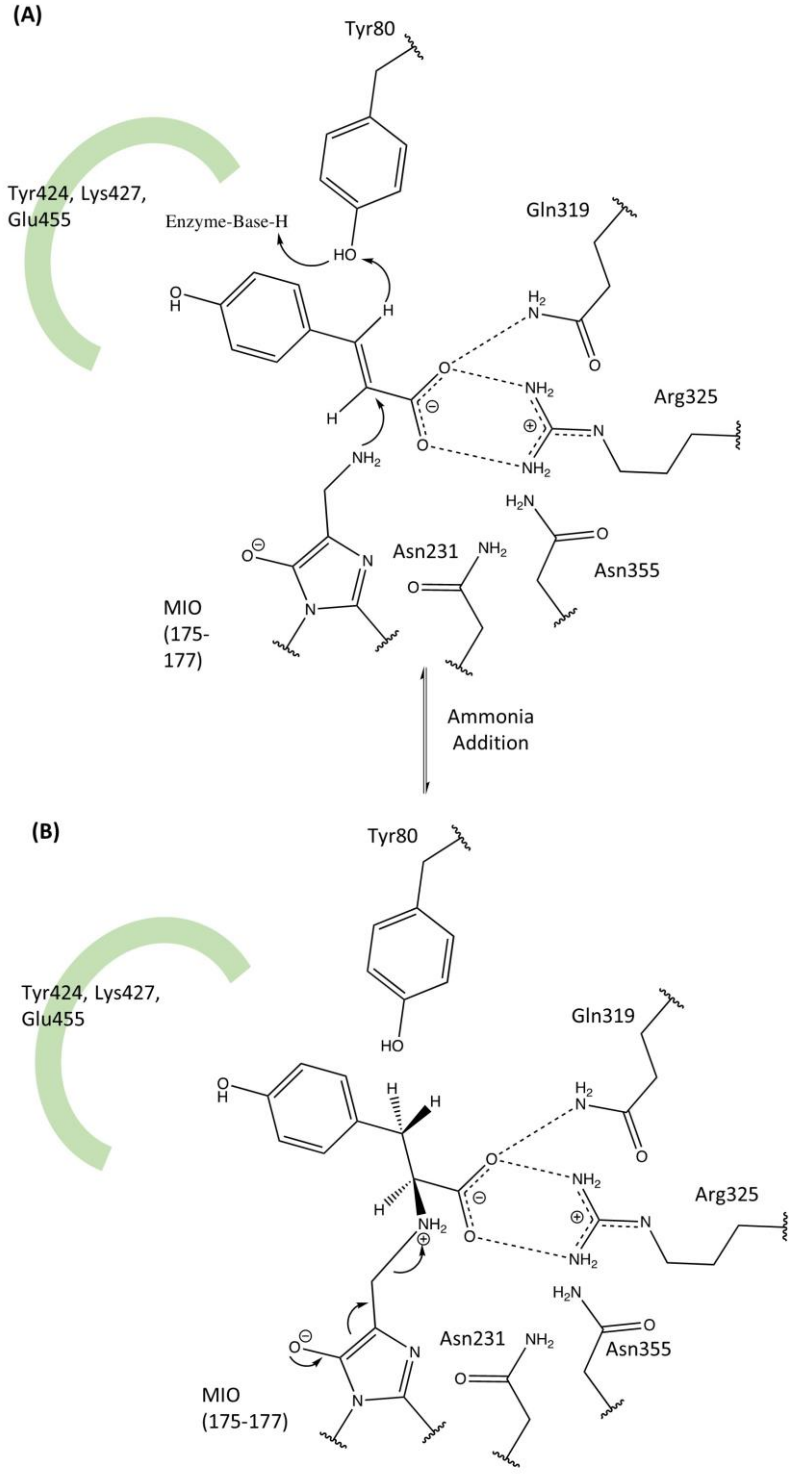

Figure 5. *Cont*.

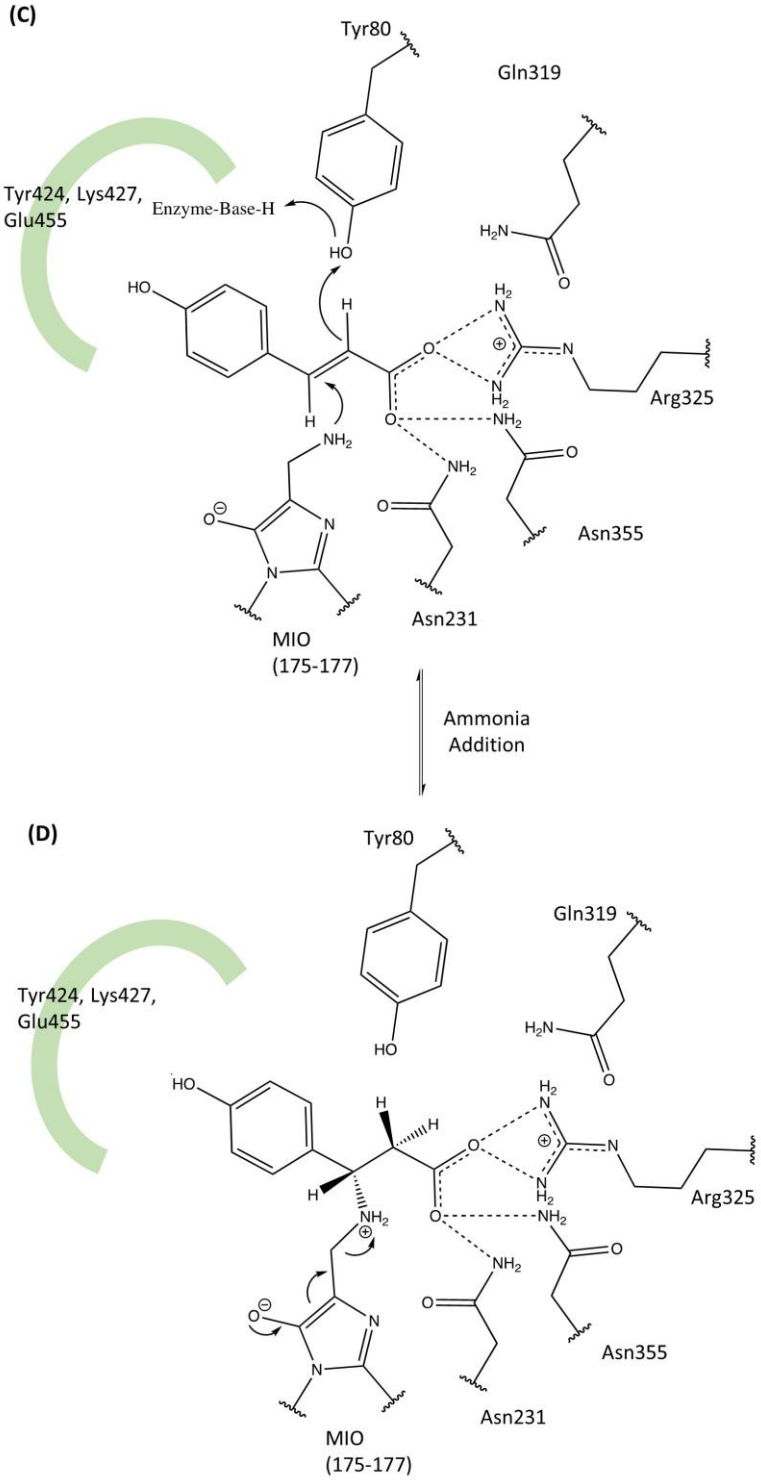

Figure 5. The proposed reaction mechanism for TchPAM during the ammonia addition of (*S*)-α-tyrosine and (*R*)-β-tyrosine in mutant Tyr424Asn as an example. (**A**) The binding mode I when *trans-p*-hydroxycinnamic acid enters the active site as substrate. (**B**) The ammonia addition on *trans-p*-hydroxycinnamic acid in the binding mode I to yield (*S*)-α-tyrosine. (**C**) The binding mode II when *trans-p*-hydroxycinnamic acid enters the active site as the substrate. (**D**) The ammonia addition on *trans-p*-hydroxycinnamic in the binding mode II to yield (*R*)-β-tyrosine.

This hypothesis was backed up by the measurement of the conversion and the enantiomeric excess of the designed enzymes in ammonia addition reaction of *trans-p*-hydroxycinnamic acid, monitored by High-performance liquid chromatography (HPLC)

assays. Both candidate mutants, where the residue was replaced by asparagine or cysteine with a smaller and different chemical functional side chain in position 424, presented the tyrosine ammonia-lyase activity (Table 2). Strikingly, the superior mutants Tyr424Asn and Tyr424Cys were designed for the generation of optically pure (*R*)-β-tyrosine. The specific activities of mutants Tyr424Asn and Tyr424Cys were 0.104 ± 0.002 and 0.141 ± 0.001 U/mg, respectively. The lack of tyrosine ammonia-lyase activity with the wild type might be ascribed to the steric clash between the aryl ring on the substrate and the residue Tyr424, while both β-selective variants provide extra space at this position. Taken together, these results strongly indicate the significance of the residues in a third binding pocket, including Tyr424, as well as its neighborhoods Lys427, Ile431, and Glu455, for substrate specificity.

Table 2. Comparison of the specific activity and enantiomeric excess of wild type and mutants Tyr424Asn and Tyr424Cys in the ammonia addition reaction.

Enzyme	Specific Activity				$ee^{\beta}{}_{R}$	Reference
	(*S*)-α-Tyrosine	**(*R*)-α-Tyrosine**	**(*S*)-β-Tyrosine**	**(*R*)-β-Tyrosine**		
Wt	n.d.	n.d.	n.d.	n.d.	-	[1]
Y424N	n.d.	n.d.	n.d.	0.104 ± 0.002	>99%	This work
Y424C	n.d.	n.d.	n.d.	0.141 ± 0.001	>99%	This work

3. Conclusions and Perspectives

With excessive consumption of natural petroleum, the option to convert the underutilized lignin into high-value products has been recognized, based on its significant potential as a sustainable source of numerous aromatic compounds. In this paper, we reported an enzymatic conversion of *trans-p*-hydroxycinnamic acid into (*R*)-β-tyrosine with high enantiopurity as a valuable building block for pharmaceutical ingredients and drug candidates, such as kedarcidin [51]. However, the synthesis of (*R*)-β-tyrosine by natural MIO-dependent enzymes remains considerably challenging because of the low enantioselectivity of bacterial tyrosine aminomutase, as well as the poor tyrosine acceptance of the phenylalanine-metabolizing enzymes [47,48]. To form the cornerstone of the whole strategy, TchPAM was chosen for mutation via computational enzyme design to extend the substrate scope, according to the previous evidence of its great synthetic potential of (*R*)-β-phenylalanine. In conclusion, the variants Tyr424Asn and Tyr424Cys were found to yield (*R*)-β-tyrosine with high enantiopurity from *trans-p*-hydroxycinnamic acid. Using this variant, efficient and straightforward routes can be demonstrated by developing high-value chiral β-amino acids, as the building blocks in bioactive natural products, from lignocellulosic waste, which comprises corresponding aromatic compounds. This could be achieved through the multi-enzymatic cascade involving the designed TchPAM and the feruloyl esterases, which are able to release *p*-hydroxycinnamic acids from lignin, enabling sequential enzymatic conversion to be performed in a one-pot synthesis method [52]. Combining the enzymatic conversion with the further downstream synthesis of bioderived anticancer drug based on the enantiopure (*R*)-β-tyrosine, we pointed out the possibility of valorization of the underused lignin in a low-molecular-weight value-added product (Figure 6).

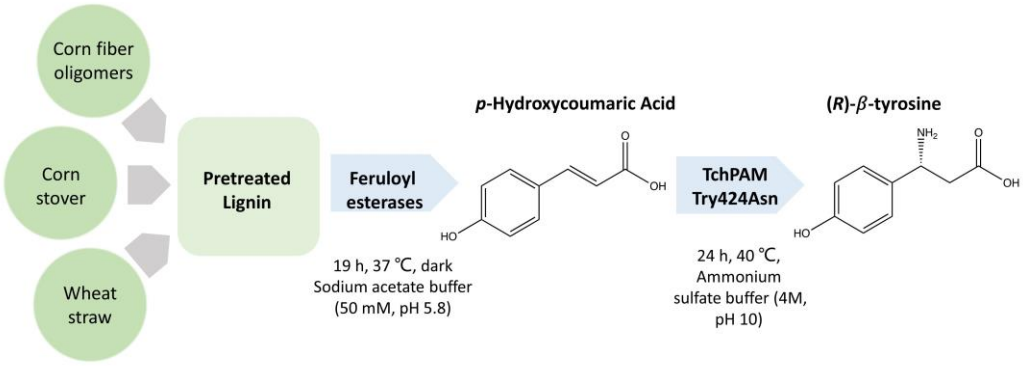

Figure 6. Proposed pathway for multi-enzymatic synthesis of (*R*)-β-tyrosine with high enantiopurity starting from the pretreated lignin.

In summary, this study highlighted a lignin-based β-tyrosine synthesis process, employing the computational-designed TchPAM. This enzymatic conversion for the production of the (*R*)-β-tyrosine with excellent enantioselectivity and regioselectivity could connect with the upstream production process of *p*-hydroxycinnamic acid from lignin, as well as the drug development downstream in pharmaceutical industries, providing meaningful opportunities for future research in lignin valorization.

4. Materials and Methods

4.1. Computational Enzyme Design

To determine the appropriate residues to mutate, the computational design of TchPAM was processed by using RosettaScripts, a scripting language interface based on PyRosetta [53]. The β-tyrosine as the target substrate and the MIO moiety were manipulated by software OpenBabel 2.4 [54] and their transition state geometry optimized in Gaussian09 [55]. Moreover, the Biology and Chemistry Library Project (BCL) was used to generate the substrate and moiety conformers [56]. According to the staring coordinates, which are determined by the information of the PDB file, the natural substrate was replaced with the prepared target substrate in the binding pocket of the relaxed enzyme (PDB ID: 4C5R). Finally, the best designs were selected based on the calculation of catalytic constraints from PyRosetta by using a high-performance computer and the structure comparison of natural templates in the visualization system PyMOL [57] and Chimera [58].

4.2. Construction of TchPAM Mutants

According to the protein sequence from *Taxus chinensis* (NCBI, AAU01182.1), the pET28a plasmid, containing the codon-optimized *pam* gene, was synthesized by ProteoGenix (Schiltigheim, France) and used as a template for site-directed mutagenesis with Q5® High-Fidelity 2X Master Mix (NEB, Ipswich, MA, USA). Apart from the mutation at residue Tyr424 with KLD Enzyme Mix from NEB (Ipswich, MA, USA), the touch-down PCR was performed for the rest of the mutants. All primers were ordered from Thermo Fischer Scientific (Waltham, MA, USA) and are listed in Supplementary Materials Table S1. The template strand was immediately removed by adding 1 µL of DpnI for 1 h at 37 °C. Subsequently, the PCR reaction mixture was transformed into high-efficiency chemically T7 express competent *E. coli* (NEB, USA), according to the manufacturer's protocol. Mutagenesis success was controlled by Sanger sequencing (GATC, Ebersberg, Germany) of purified plasmid from the well-isolated colonies.

4.3. Expression, Purification, and Concentration of TchPAM

For the expression of the wild type and the mutants of TchPAM, the cells were incubated in 100 mL of LB-medium with 50 µg/mL kanamycin at 37 °C and 120 rpm. Once the OD_{600} reached 0.3–0.4, the cultures were induced with 0.1 mM IPTG at 25 °C with shaking at 120 rpm. After 22 h, cells were harvested by centrifugation, washed twice

with 50 mM Tris-HCl buffer (pH 8.0), and resuspended in 5 mL of binding buffer (50 mM Tris-HCl, 150 mM NaCl, 10 mM imidazole, pH 8.0). Cell disruption was performed on ice by sonication (20 s pulse/30 s pause over 10 min, with 40 % amplitude, HD3100, Bandelin electronic GmbH & Co. KG, Berlin, Germany). Cell debris was removed by centrifugation (16,000× *g*, 20 min, 4 °C) (Megafuge 40R, Thermo Fisher Scientific Inc., Waltham, MA, USA). The histidine-tagged enzymes were obtained through purification with His SpinTrap columns (GE Healthcare Life Sciences, London, UK). The composition of the washing buffer (pH 8.0) was 50 mM Tris-HCl, 150 mM NaCl, and 20 mM imidazole, while the elution buffer had the same composition except for a higher concentration of imidazole (300 mM). Then, the purified enzymes were desalted and concentrated by the protein concentrators with a 10 K MWCO (Pierce® Concentrator, PES, 0.5 mL, Thermo Fisher Scientific Inc., Waltham, MA, USA). Finally, the protein concentrations of the wild type and mutants of TchPAM were determined by using the Epoch™ Multi-volume Spectrophotometer System (BioTek Instruments, Inc., Winusky, VT, USA) with a Take3Plate (BioTek Instruments, Inc., Winusky, VT, USA), based on the BSA protocol. All purified enzyme solutions were diluted to 0.5 mg/mL as enzyme stock for subsequent activity measurement. The purity of the desalted enzymes was checked by SDS-PAGE (Supplementary Materials Figure S1).

4.4. TchPAM Activity Assays for Ammonia Elimination Reactions

The substrate solution of 1 mM substrate ((*S*)-α-phenylalanine, (*R*)-β-phenylalanine, (*S*)-α-tyrosine, or (*R*)-β-tyrosine) was prepared in Tris-HCl buffer (50 mM, pH 8.8) and pipetted in 96-well UV-Microplates. Then, 10 µL of purified wild type or mutant TchPAM enzyme were added to the preheated 100 µL of substrate solution. The ammonia elimination reactions were carried out in triplicate at 40 °C for 30 min, monitoring the product absorbance for *trans*-cinnamic acid at 300 nm, as well as for *trans-p*-hydroxycinnamic acid at 350 nm. The product absorbance was measured every 3 min by using the Epoch™ Spectrophotometer system (BioTek, Winusky, VT, USA).

4.5. Kinetics Measurements

The above-mentioned protocol was used to determine the kinetic parameters of the wild type and mutants of TchPAM. The measurements were performed in triplicate in 96-well UV-Microplates, with a varying substrate concentration range between 0.01 and 10 mM, until substrate saturation occurred. The maximal concentration of (*S*)-α-tyrosine was 2 mM due to its poor solubility in Tris-HCl buffer (pH 8.8). The kinetic parameters (K_M and V_{max}) were determined by employing Michaelis–Menten nonlinear fitting using Origin (Pro 2019, OriginLab®, Northampton, MA, USA).

4.6. HPLC Analysis in the Ammonia Addition Reaction

Substrate solution with 3 mM *trans-p*-hydroxycinnamic acids was prepared in ammonium sulfate solution (4 M, pH 10). First, 50 µL of purified enzymes were added to 500 µL of substrate solution. The reaction was performed at 40 °C. After the indicated reaction time (0, 1, 2, 3, 5, 7, and 24 h), 50 µL of sample were taken from the mixture and heated at 99 °C for 5 min. To determine the concentration of all four mentioned aromatic amino acids, which are possible products of the reaction, the samples were analyzed by HPLC (1200 Series, Agilent Technologies, Waldbronn, Germany). Then, 0.5 µL of sample were injected in the HPLC column (C18, 150 × 4.6 mm HyperClone 5 µm, Phenomenex Inc, Aschaffenburg, Germany) after derivatization with *o*-phthalaldehyde (OPA) and *N*-isobutyryl-L-cysteine (IBLC) in an automatic pre-column according to the protocol by Brucher et al. [59]. The compounds in the reaction mixture were eluted with 21% sodium phosphate buffer (40 mM, pH 6.5) and 79 % methanol at a constant flow rate of 1 min/mL. The detector was operated at 338 nm. The retention times of the produced aromatic amino acids were (*S*)-α-tyrosine 71.0 min, (*R*)-α-tyrosine 45.7 min, (*S*)-β-tyrosine 57.6 min, and (*R*)-β-tyrosine 42.7 min.

Supplementary Materials: The following are available online at https://www.mdpi.com/article/10.3390/catal11111310/s1, Supplementary Table S1: The list of primers for site-directed mutagenesis through touch down method; Supplementary Table S2: The list of primers for site-directed mutagenesis through KLD (Kinase, Ligase, and DpnI enzymes) method. Supplementary Figure S1: The SDS-PAGE gel of the crude protein lysate and purified enzymes. The band of TchPAM was observed between 63 and 75 kDa. WT: wild type.

Author Contributions: Conceptualization, J.R.; methodology, U.E. and F.P.; high performance computer, H.A.; computational enzyme design, screening the designed enzyme, characterization of the enzyme by UV spectroscopy and HPLC, F.P.; writing the manuscript, F.P.; revising the manuscript, J.R., U.E., A.D. and H.A.; supervision, J.R. All authors have read and agreed to the published version of the manuscript.

Funding: This work by author was supported by China Scholarship Council and is part of the bioeconomy graduate program BBW ForWerts. We gratefully thank the Open Access Publishing Fund of Karlsruhe Institute of Technology.

Conflicts of Interest: The authors declare no conflict of interest.

References

1. Islam, M.R.; Hossain, M.E. Chapter 1—Introduction. In *Drilling Engineering*; Islam, M.R., Hossain, M.E., Eds.; Sustainable Oil and Gas Development Series; Gulf Professional Publishing: Houston, TX, USA, 2021; pp. 1–16. ISBN 978-0-12-820193-0.
2. Ge, X.; Chang, C.; Zhang, L.; Cui, S.; Luo, X.; Hu, S.; Qin, Y.; Li, Y. Chapter Five—Conversion of Lignocellulosic Biomass Into Platform Chemicals for Biobased Polyurethane Application. In *Advances in Bioenergy*; Li, Y., Ge, X., Eds.; Elsevier: Amsterdam, The Netherlands, 2018; Volume 3, pp. 161–213.
3. Yousuf, A.; Pirozzi, D.; Sannino, F. Chapter 1—Fundamentals of lignocellulosic biomass. In *Lignocellulosic Biomass to Liquid Biofuels*; Yousuf, A., Pirozzi, D., Sannino, F., Eds.; Academic Press: Cambridge, MA, USA, 2020; pp. 1–15. ISBN 978-0-12-815936-1.
4. Gutiérrez-Antonio, C.; Romero-Izquierdo, A.G.; Gómez-Castro, F.I.; Hernández, S. 5—Production processes from lignocellulosic feedstock. In *Production Processes of Renewable Aviation Fuel*; Gutiérrez-Antonio, C., Romero-Izquierdo, A.G., Gómez-Castro, F.I., Hernández, S., Eds.; Elsevier: Amsterdam, The Netherlands, 2021; pp. 129–169. ISBN 978-0-12-819719-6.
5. Abdel-Hamid, A.M.; Solbiati, J.O.; Cann, I.K. Insights into lignin degradation and its potential industrial applications. *Adv. Appl. Microbiol.* **2013**, *82*, 1–28.
6. Thomas, B.; Murphy, D.J.; Murray, B.G. *Encyclopedia of Applied Plant Sciences*; Academic Press: Cambridge, MA, USA, 2016.
7. Demuner, I.F.; Colodette, J.L.; Demuner, A.J.; Jardim, C.M. Biorefinery review: Wide-reaching products through kraft lignin. *BioResources* **2019**, *14*, 7543–7581. [CrossRef]
8. Mahmood, N.; Yuan, Z.; Schmidt, J.; Xu, C. (Charles) Depolymerization of lignins and their applications for the preparation of polyols and rigid polyurethane foams: A review. *Renew. Sustain. Energy Rev.* **2016**, *60*, 317–329. [CrossRef]
9. Bengtsson, A.; Bengtsson, J.; Sedin, M.; Sjöholm, E. Carbon Fibers from Lignin-Cellulose Precursors: Effect of Stabilization Conditions. *ACS Sustain. Chem. Eng.* **2019**, *7*, 8440–8448. [CrossRef]
10. Ghaffar, S.H.; Fan, M. Lignin in straw and its applications as an adhesive. *Int. J. Adhes. Adhes.* **2014**, *48*, 92–101. [CrossRef]
11. Yuliestyan, A.; García-Morales, M.; Moreno, E.; Carrera, V.; Partal, P. Assessment of modified lignin cationic emulsifier for bitumen emulsions used in road paving. *Mater. Des.* **2017**, *131*, 242–251. [CrossRef]
12. Zhou, M.; Wang, D.; Peng, R.; Yang, D.; Qiu, X.; Qian, Y. Synthesis of a Hindered Amine-Grafted Lignin-Based Emulsifier and Its Application in a Green Emulsifiable Concentrate. *J. Agric. Food Chem.* **2019**, *67*, 11129–11136. [CrossRef]
13. Gravitis, J.; Abolinš, J.; Tupčiauskas, R.; Veveris, A. Lignin from steam-exploded wood as binder in wood composites. *J. Environ. Eng. Landsc. Manag.* **2010**, *18*, 75–84. [CrossRef]
14. Xie, S.; Li, Q.; Karki, P.; Zhou, F.; Yuan, J.S. Lignin as Renewable and Superior Asphalt Binder Modifier. *ACS Sustain. Chem. Eng.* **2017**, *5*, 2817–2823. [CrossRef]
15. Chauhan, P.S. Lignin nanoparticles: Eco-friendly and versatile tool for new era. *Bioresour. Technol. Rep.* **2020**, *9*, 100374. [CrossRef]
16. Takada, M.; Rabemanolontsoa, H.; Minami, E.; Saka, S. Characterization of lignin-derived products from various lignocellulosics as treated by semi-flow hot-compressed water. *J. Wood Sci.* **2018**, *64*, 802–809. [CrossRef]
17. Plesu Popescu, A.E.; Torralba, J.; Bonet, J.; Llorens, J. Vanillin production from lignin: Rigorous process simulation results for ethyl acetate versus aliphatic-alcohol-specific process designs. *Clean. Eng. Technol.* **2021**, *4*, 100133. [CrossRef]
18. Beckham, G.T. *Lignin Valorization: Emerging Approaches*; Royal Society of Chemistry: London, UK, 2018.
19. Becker, J.; Wittmann, C. A field of dreams: Lignin valorization into chemicals, materials, fuels, and health-care products. *Biotechnol. Adv.* **2019**, *37*, 107360. [CrossRef] [PubMed]
20. Li, M.; Li, Y.; Zhang, W.; Li, S.; Gao, Y.; Ai, X.; Zhang, D.; Liu, B.; Li, Q. Metabolomics analysis reveals that elevated atmospheric CO2 alleviates drought stress in cucumber seedling leaves. *Anal. Biochem.* **2018**, *559*, 71–85. [CrossRef] [PubMed]
21. Sarker, U.; Oba, S. Augmentation of leaf color parameters, pigments, vitamins, phenolic acids, flavonoids and antioxidant activity in selected Amaranthus tricolor under salinity stress. *Sci. Rep.* **2018**, *8*, 12349. [CrossRef]

22. Wang, J.; Yuan, B.; Huang, B. Differential heat-induced changes in phenolic acids associated with genotypic variations in heat tolerance for hard fescue. *Crop Sci.* **2019**, *59*, 667–674. [CrossRef]
23. Baleroni, C.R.S.; Ferrarese, M.L.L.; Souza, N.E.; Ferrarese-Filho, O. Lipid accumulation during canola seed germination in response to cinnamic acid derivatives. *Biol. Plant.* **2000**, *43*, 313–316. [CrossRef]
24. Timokhin, V.I.; Regner, M.; Motagamwala, A.H.; Sener, C.; Karlen, S.D.; Dumesic, J.A.; Ralph, J. Production of p-Coumaric Acid from Corn GVL-Lignin. *ACS Sustain. Chem. Eng.* **2020**, *8*, 17427–17438. [CrossRef]
25. Marques, G.; Gutiérrez, A.; Del Río, J.C. Chemical characterization of lignin and lipophilic fractions from leaf fibers of curaua (Ananas erectifolius). *J. Agric. Food Chem.* **2007**, *55*, 1327–1336. [CrossRef] [PubMed]
26. WHO. 2020. Available online: https://www.who.int/news-room/fact-sheets/detail/cancer (accessed on 30 September 2021).
27. Christianson, C.V.; Montavon, T.J.; Van Lanen, S.G.; Shen, B.; Bruner, S.D. The structure of L-tyrosine 2,3-aminomutase from the C-1027 enediyne antitumor antibiotic biosynthetic pathway. *Biochemistry* **2007**, *46*, 7205–7214. [CrossRef]
28. Malik, S.; Cusidó, R.M.; Mirjalili, M.H.; Moyano, E.; Palazón, J.; Bonfill, M. Production of the anticancer drug taxol in Taxus baccata suspension cultures: A review. *Process Biochem.* **2011**, *46*, 23–34. [CrossRef]
29. Gond, S.K.; Kharwar, R.N.; White, J.F. Will fungi be the new source of the blockbuster drug taxol? *Fungal Biol. Rev.* **2014**, *28*, 77–84. [CrossRef]
30. Baedeker, M.; Schulz, G.E. Autocatalytic peptide cyclization during chain folding of histidine ammonia-lyase. *Structure* **2002**, *10*, 61–67. [CrossRef]
31. Sánchez-Murcia, P.A.; Bueren-Calabuig, J.A.; Camacho-Artacho, M.; Cortés-Cabrera, Á.; Gago, F. Stepwise Simulation of 3,5-Dihydro-5-methylidene-4H-imidazol-4-one (MIO) Biogenesis in Histidine Ammonia-lyase. *Biochemistry* **2016**, *55*, 5854–5864. [CrossRef]
32. Sharma, A.; Shahzad, B.; Rehman, A.; Bhardwaj, R.; Landi, M.; Zheng, B. Response of phenylpropanoid pathway and the role of polyphenols in plants under abiotic stress. *Molecules* **2019**, *24*, 2452. [CrossRef]
33. Wu, B.; Szymański, W.; Wybenga, G.G.; Heberling, M.M.; Bartsch, S.; Dewildeman, S.; Poelarends, G.J.; Feringa, B.L.; Dijkstra, B.W.; Janssen, D.B. Mechanism-inspired engineering of phenylalanine aminomutase for enhanced β-regioselective asymmetric amination of cinnamates. *Angew. Chem. Int. Ed.* **2012**, *51*, 482–486. [CrossRef]
34. Wybenga, G.G.; Szymanski, W.; Wu, B.; Feringa, B.L.; Janssen, D.B.; Dijkstra, B.W. Structural investigations into the stereochemistry and activity of a phenylalanine-2,3-aminomutase from Taxus chinensis. *Biochemistry* **2014**, *53*, 3187–3198. [CrossRef] [PubMed]
35. Tinberg, C.E.; Khare, S.D.; Dou, J.; Doyle, L.; Nelson, J.W.; Schena, A.; Jankowski, W.; Kalodimos, C.G.; Johnsson, K.; Stoddard, B.L.; et al. Computational design of ligand-binding proteins with high affinity and selectivity. *Nature* **2013**, *501*, 212–216. [CrossRef]
36. Wu, B.; Szymanski, W.; Wietzes, P.; de Wildeman, S.; Poelarends, G.J.; Feringa, B.L.; Janssen, D.B. Enzymatic synthesis of enantiopure α- and β-amino acids by phenylalanine aminomutase-catalysed amination of cinnamic acid derivatives. *ChemBioChem* **2009**, *10*, 338–344. [CrossRef]
37. Watts, K.T.; Mijts, B.N.; Lee, P.C.; Manning, A.J.; Schmidt-Dannert, C. Discovery of a Substrate Selectivity Switch in Tyrosine Ammonia-Lyase, a Member of the Aromatic Amino Acid Lyase Family. *Chem. Biol.* **2006**, *13*, 1317–1326. [CrossRef] [PubMed]
38. Hou, Q.; Bourgeas, R.; Pucci, F.; Rooman, M. Computational analysis of the amino acid interactions that promote or decrease protein solubility. *Sci. Rep.* **2018**, *8*, 14661. [CrossRef]
39. Burley, S.K.; Petsko, G.A. Amino-aromatic interactions in proteins. *FEBS Lett.* **1986**, *203*, 139–143.
40. Lin, F.Y.; MacKerell, A.D. Improved Modeling of Cation-π and Anion-Ring Interactions Using the Drude Polarizable Empirical Force Field for Proteins. *J. Comput. Chem.* **2020**, *41*, 439–448. [CrossRef] [PubMed]
41. Biot, C.; Buisine, E.; Kwasigroch, J.M.; Wintjens, R.; Rooman, M. Probing the energetic and structural role of amino acid/nucleobase cation-π interactions in protein-ligand complexes. *J. Biol. Chem.* **2002**, *277*, 40816–40822. [CrossRef] [PubMed]
42. Philip, V.; Harris, J.; Adams, R.; Nguyen, D.; Spiers, J.; Baudry, J.; Howell, E.E.; Hinde, R.J. A Survey of Aspartate À Phenylalanine and Glutamate À Phenylalanine. *Biochemistry* **2011**, *50*, 2939–2950. [CrossRef]
43. McGaughey, G.B.; Gagné, M.; Rappé, A.K. π-Stacking interactions. Alive and well in proteins. *J. Biol. Chem.* **1998**, *273*, 15458–15463. [CrossRef] [PubMed]
44. Janiak, C. A critical account on n-n stacking in metal complexes with aromatic nitrogen-containing ligands. *J. Chem. Soc. Dalt. Trans.* **2000**, 3885–3896. [CrossRef]
45. Feng, L.; Wanninayake, U.; Strom, S.; Geiger, J.; Walker, K.D. Mechanistic, mutational, and structural evaluation of a taxus phenylalanine aminomutase. *Biochemistry* **2011**, *50*, 2919–2930. [CrossRef]
46. Tork, S.D.; Nagy, E.Z.A.; Cserepes, L.; Bordea, D.M.; Nagy, B.; Toşa, M.I.; Paizs, C.; Bencze, L.C. The production of l- and d-phenylalanines using engineered phenylalanine ammonia lyases from Petroselinum crispum. *Sci. Rep.* **2019**, *9*, 20123. [CrossRef]
47. Rachid, S.; Krug, D.; Weissman, K.J.; Müller, R. Biosynthesis of (R)-β-tyrosine and its incorporation into the highly cytotoxic chondramides produced by Chondromyces crocatus. *J. Biol. Chem.* **2007**, *282*, 21810–21817. [CrossRef] [PubMed]
48. Krug, D.; Müller, R. Discovery of additional members of the tyrosine aminomutase enzyme family and the mutational analysis of CmdF. *ChemBioChem* **2009**, *10*, 741–750. [CrossRef]

49. Yan, J.; Aboshi, T.; Teraishi, M.; Strickler, S.R.; Spindel, J.E.; Tung, C.-W.; Takata, R.; Matsumoto, F.; Maesaka, Y.; McCouch, S.R.; et al. The Tyrosine Aminomutase TAM1 Is Required for β-Tyrosine Biosynthesis in Rice. *Plant Cell* **2015**, *27*, 1265–1278. [CrossRef] [PubMed]
50. Deruiter, J. Carboxylic Acid Structure and Chemistry: Part 1. *Princ. Drug Action* **2005**, *1*, 1–11.
51. Carretero-Molina, D.; Ortiz-Lopez, F.J.; Martín, J.; González, I.; Sánchez-Hidalgo, M.; Román-Hurtado, F.; Díaz, C.; de la Cruz, M.; Genilloud, O.; Reyes, F. Pentaminomycins F and G, first non-ribosomal peptides containing 2-pyridylalanine. *J. Nat. Prod.* **2021**, *84*, 1–27. [CrossRef] [PubMed]
52. Underlin, E.N.; Frommhagen, M.; Dilokpimol, A.; van Erven, G.; de Vries, R.P.; Kabel, M.A. Feruloyl Esterases for Biorefineries: Subfamily Classified Specificity for Natural Substrates. *Front. Bioeng. Biotechnol.* **2020**, *8*, 332. [CrossRef] [PubMed]
53. Chaudhury, S.; Lyskov, S.; Gray, J.J. PyRosetta: A script-based interface for implementing molecular modeling algorithms using Rosetta. *Bioinformatics* **2010**, *26*, 689–691. [CrossRef]
54. Boyle, N.M.O.; Banck, M.; James, C.A.; Morley, C.; Vandermeersch, T.; Hutchison, G.R. Open Babel: An open chemical toolbox. *J. Cheminform.* **2011**, *3*, 33. [CrossRef]
55. Frisch, M.J.; Trucks, G.W.; Schlegel, H.B.; Scuseria, G.E.; Robb, M.A.; Cheeseman, J.R.; Scalmani, G.; Barone, V.; Petersson, G.A.; Nakatsuji, H.; et al. *Gaussian 09, Revision A.02*; Gaussian, Inc: Wallingford, CT, USA, 2016.
56. BCL. Available online: http://www.meilerlab.org/index.php/servers/bcl-academic-license (accessed on 30 September 2021).
57. Schrödinger, LLC. *The {PyMOL} Molecular Graphics System, Version~1.8*; Schrödinger, LLC: Portland, OR, USA, 2015.
58. Pettersen, E.F.; Goddard, T.D.; Huang, C.C.; Couch, G.S.; Greenblatt, D.M.; Meng, E.C.; Ferrin, T.E. UCSF Chimera—a visualization system for exploratory research and analysis. *J. Comput. Chem.* **2004**, *25*, 1605–1612. [CrossRef]
59. Brückner, H.; Wittner, R.; Godel, H. Automated enantioseparation of amino acids by derivatization with o-phthaldialdehyde and n-acylated cysteines. *J. Chromatogr.* **1989**, *476*, 73–82. [CrossRef]